Extramedullary Chitosan Channels Promote Survival of Transplanted Neural Stem and Progenitor Cells and Create a Tissue Bridge After Complete Spinal Cord Transection

HIROSHI NOMURA, M.D., Ph.D.,[1] TASNEEM ZAHIR, Ph.D.,[2–4] HOWARD KIM,[4,5]
YUSUKE KATAYAMA, MASc.,[6] IRIS KULBATSKI, Ph.D.,[1] CINDI M. MORSHEAD, Ph.D.,[5,7,8]
MOLLY S. SHOICHET, Ph.D.,[2–4,8] and CHARLES H. TATOR, M.D., Ph.D.[1]

ABSTRACT

Transplantation of neural stem and progenitor cells (NSPCs) is a promising strategy for repair after spinal cord injury. However, the epicenter of the severely damaged spinal cord is a hostile environment that results in poor survival of the transplanted NSPCs. We examined implantation of extramedullary chitosan channels seeded with NSPCs derived from transgenic green fluorescent protein (GFP) rats after spinal cord transection (SCT). At 14 weeks, we assessed the survival, maturation, and functional results using NSPCs harvested from the brain (brain group) or spinal cord (SC group) and seeded into chitosan channels implanted between the cord stumps after complete SCT. Control SCT animals had empty chitosan channels or no channels implanted. Channels seeded with brain or spinal cord–derived NSPCs showed a tissue bridge, although the bridges were thicker in the brain group. Both cell types showed long-term survival, but the number of surviving cells in the brain group was approximately five times as great as in the SC group. In both the brain and SC groups at 14 weeks after transplantation, many host axons were present in the center of the bridge in association with the transplanted cells. At 14 weeks astrocytic and oligodendrocytic differentiation in the channels was 24.8% and 17.3%, respectively, in the brain group, and 31.8% and 9.7%, respectively, in the SC group. The channels caused minimal tissue reaction in the adjacent spinal cord. There was no improvement in locomotor function. Thus, implantation of chitosan channels seeded with NSPCs after SCT created a tissue bridge containing many surviving transplanted cells and host axons, although there was no functional improvement.

INTRODUCTION

NEURAL STEM AND PROGENITOR CELLS (NSPCs) are multipotential cells capable of self-renewing and differentiating into mature neural cells such as astrocytes, oligodendrocytes, and neurons.[1] Transplantation of NSPCs is one of the most promising experimental strategies for repair of spinal cord injury (SCI),[1,2] and some human trials have been undertaken.[3] However, there has been poor survival of the transplanted NSPCs in the adult central nervous system (CNS), especially at the injury epicenter. Additional measures such as the application of neurotrophic factors or immunosuppression are necessary to enhance the viability of the transplanted NSPCs.[4–7] Furthermore, it may be

[1]Toronto Western Research Institute, Toronto Western Hospital, Toronto, Ontario, Canada.
[2]Department of Chemical Engineering and Applied Chemistry, [3]Department of Chemistry, [4]Institute of Biomaterials and Biomedical Engineering, and [5]Institute of Medical Sciences, University of Toronto, Toronto, Ontario, Canada.
[6]matREGEN, Toronto, Ontario, Canada.
[7]Department of Surgery, and [8]Terrence Donnelly Center for Cellular and Biomolecular Research, University of Toronto, Toronto, Ontario, Canada.

important to provide the NSPCs with a 3-dimensional (3D) scaffold to anchor the cells at the lesion site and allow them to differentiate into mature cells. Although several studies using artificial or biological scaffolds seeded with NSPCs have been reported in experimental CNS injury,[8–11] the injuries were of only mild to moderate severity, which may have aided long-term survival of the transplanted cells. To our knowledge, there have been no reports of the use of artificial scaffolds in combination with transplanted NSPCs after complete spinal cord transection (SCT), the most severe experimental SCI.

Our group has focused on the application of bioengineering techniques using synthetic guidance channels to promote axonal regeneration across the lesion site and to reduce the barrier caused by scar tissue. We have also used local drug delivery systems to administer neuroprotective or regenerative agents directly into the epicenter of the damaged spinal cord.[12–20] In general, there are three types of artificial scaffolds for experimental SCI: gels, sponges, and channels.[2,21] Channels have the advantage of providing a directional pathway or bridge for axonal regrowth across the lesion. We previously reported implantation of synthetic hydrogel guidance channels made of poly(2-hydroxyethyl methacrylate-comethyl methacrylate), a frequently used nonbiodegradable material (e.g., in soft contact lenses) to promote a tissue bridge containing regenerating axons between the stumps after complete SCT. However, the bridges were small and contained few regenerating axons.[15–17] There were also side effects, including caudal migration of the rostral stump and syringomyelia, possibly due to subarachnoid scarring. Currently, we are focusing on channels composed of chitosan, a biodegradable polysaccharide.[12,22] Several recent *in vitro* studies have demonstrated high biocompatibility of chitosan substrates for neural[23] or mesenchymal stem cells.[24] We hypothesized that implantation of chitosan channels seeded with NSPCs after SCT would permit long-term survival of the transplanted cells.

Recently, our group reported the differentiation of adult rat brain–derived NSPCs cultured on laminin-coated tissue culture slides for 7 days or chitosan matrices for 48 hours *in vitro* and a preliminary *in vivo* trial of the NSPCs seeded on chitosan channels after channel implantation in SCT. We found excellent survival and neural differentiation of the cells at 5 weeks.[25] The present study examines the long-term survival and differentiation of the NSPCs on chitosan channels *in vivo* and the morphological and functional effects of the strategy of implantation of chitosan channels seeded with NSPCs after SCT.

It is not known which NSPCs are most useful for SCI; the choices include embryonic, fetal or adult cells derived from the brain or spinal cord.[1] Our group has concentrated on adult NSPCs harvested from the periventricular region of the spinal cord of adult rats[26–28] because they are more terminally differentiated and represent the population of cells requiring replacement at the injury site. Recently, it was reported that transplantation of adult rat spinal cord–derived NSPCs into the adult rat spinal cord after weight-drop injury achieved significant recovery of hindlimb locomotor function and sensory responses,[29] and other investigators have reported that transplanted adult brain–derived NSPCs promote neurogenesis.[30–32] In SCI, there has been no comparative study of cell survival, differentiation, or functional recovery between brain- and spinal cord–derived NSPCs.

In the present study, we examined implantation after SCT of extramedullary chitosan channels seeded with NSPCs derived from the brain or spinal cord of adult transgenic Wistar rats expressing the gene for enhanced green fluorescent protein (GFP). We compared the survival and differentiation profile of these two populations of NSPCs and examined their effect on locomotor recovery in Sprague-Dawley rats.

MATERIALS AND METHODS

Production of channels

The chitosan channels were produced as previously reported.[12] In this study, we used an 8-mm-diameter glass mold cored with a 4-mm-diameter stainless steel rod, resulting in channels approximately 4.1 mm in outer diameter and a wall thickness of 0.2 mm. For deacetylation, the channels were heated at 110°C in aqueous sodium hydroxide solution for three cycles, each for 2 h, and washed with distilled water after each cycle to achieve 92% deacetylation. The channels were cut into 10-mm lengths. Five g of medical-grade chitosan (PROTOSAN UP CL 213, Nova-Matrix, Brakeroya, Drammen, Norway) was dissolved in 500 mL of distilled water, and then the chitosan solution was precipitated using 40 mL of 4% w/w of sodium hydroxide (NaOH). Precipitated chitosan flakes were filtered and rinsed several times with distilled water until neutralization. After freeze-drying, the chitosan solution was prepared by dissolving 3% w/w chitosan in 2% v/v acetic acid. Then, 2.5 mL of the solution was mixed vigorously with 2.5 mL of ethanol and stored at 4°C, and 91 µL of acetic anhydride was added to the previous chitosan solution (5 mL total). The mixture was stirred, degassed, and injected into a glass mold (8 mm in diameter, 27 cm in length) cored with a stainless steel rod (4 mm in diameter, 27 cm in length), and after injection, the glass mold was allowed to set for 24 h to allow conversion of chitosan into a chitin hydrogel. The gelled chitin tube was removed from the core's mold and then washed vigorously with distilled water to remove excess acetic acid byproduct. The washed chitin channel was then removed from the 4-mm glass tubes, placed in 3.7-mm glass tubes, and deacetylated (to convert chitin to chitosan) using 40% w/v of NaOH. For deacetylation, the channels were heated at 110°C in the sodium hydroxide solution for three cycles, each for 2 h, and washed with distilled water after each cycle of deacetylation to achieve 92% deacetylation. The chitosan channels were then washed thoroughly with distilled water until pH = 7 and

removed from the 3.7-mm mold. The channels were dried in air for approximately 1 h and then rewetted before removing them from the mold. The channels were cut into 10-mm lengths, dried, and then sterilized using ethylene oxide gas. The channels were approximately 4.1 mm in outer diameter, and the wall thickness was 0.2 mm.

Isolation and culture of brain- or spinal cord–derived neurospheres

All NSPCs were harvested from adult enhanced GFP transgenic Wistar male rats (strain; Wistar-TgN(CAG-GFP)184ys, bred in the laboratory of Dr. A. Keating, Toronto, Canada, 200–360 g, originally obtained from the YS Institute, Inc., Utsunomiya, Tochigi, Japan).[33]

GFP transgenic rats were sacrificed, and the whole brain and cervical spinal cord were excised as described.[25,34] Brain- and spinal cord–derived neurospheres were isolated from the subependymal region of the lateral ventricles[25,35,36] and spinal cord,[34,37] respectively, and then cultured.[34,37]

Seeding of NSPCs into the inner lumen of the channels

To ensure adherence of the cells to the channel walls, sterile chitosan channels were coated with 5 μg/mL of laminin solution (Invitrogen, Burlington, ON, Canada), transferred into 24-well tissue culture plates, and incubated in complete medium overnight, before cell seeding. The next day, brain- or spinal cord–derived GFP-positive neurospheres from passage 4 cultures were centrifuged at 1500 rpm for 5 min to obtain a cell pellet and then resuspended in a small volume of complete medium (200–300 μL based on the cell count of viable cells performed on a sample of dissociated cells from the same flask) to yield a solution with a cell density of $3 \times 10^6/100$ μL. Next, the chitosan channels were transferred into empty wells, and the medium inside the channels replaced with 100 μL of cell suspension. The channels containing the neurospheres were then placed in a humidified incubator at 37°C for 1 h and rotated manually every 15 min to yield a uniform distribution of neurospheres within the channels. The seeded channels were then transferred to new wells containing complete medium and incubated for 2 days before implantation into rats with SCT.

Animals

Forty-six adult female Sprague-Dawley rats (Charles River, St. Constant, Quebec, Canada, 200–320 g) were used in this study. The Animal Care Committee of the Research Institute of the University Health Network approved the animal protocols in accordance with policies established by the Canadian Council on Animal Care. The rats with SCT were divided into 4 groups: the brain group had implantation of the laminin-coated chitosan channels seeded with adult rat brain–derived NSPCs followed by spinal fusion ($n = 11$);

the SC group was identical to the brain group, except spinal cord–derived NSPCs were seeded ($n = 12$); the empty-channel group received implantation of an empty laminin-coated channel followed by spinal fixation ($n = 12$); and the no–channel group had complete SCT followed by spinal fusion but without implantation of a channel ($n = 11$). All animals were maintained for 14 weeks after SCT.

Channel implantation

Channels were implanted after SCT at the level of T8, and spinal fixation was performed as shown Figure 1A and B and previously described.[17] The no-channel group had SCT only. To aid transplant survival, all animals were immunosuppressed daily until sacrifice with cyclosporine (15 mg/kg, Sandimmune, Novartis Pharmaceuticals Canada Inc., Dorval, QC, Canada) injected subcutaneously. Three blinded observers analyzed functional recovery weekly during the 12-week survival period using the Basso, Beattie, Bresnahan (BBB) open field locomotor test,[37] and all animals were scored for 4 min every week.

Anterograde axonal tracing with biotin dextran amine

To visualize axons from the corticospinal tract, anterograde axonal tracing with biotinylated dextran amine (BDA) was performed 12 weeks after channel implantation after completion of the behavior analysis. Three or four animals per group were randomly selected, and BDA was applied, as described previously.[17] Animals were allowed to survive for 2 more weeks before they were euthanized. The spinal cords were removed and immersed in 30% sucrose in 0.1 M phosphate buffer at 4°C for frozen sections.

Tissue preparation

Fourteen weeks after channel implantation, the rats were perfused with 4% paraformaldehyde, as described previously.[17] A 2-cm length of spinal cord encompassing the implanted channel or transection site in the no-channel group was carefully removed. The spinal cords from non—BDA-injected rats were randomly allocated for immunohistochemistry of paraffin-embedded sections, or axon counts. The spinal cords from BDA-injected rats were used for immunohistochemistry in frozen sections. The chitosan channels deteriorated in 10% neural buffered formalin and were fragmented during sectioning of paraffin-embedded tissues. Thus, the attached channels were removed from the spinal cords, and then paraffin sectioning was performed as described.[17] Every eighth or ninth section was stained with Luxol Fast Blue and hematoxylin and eosin (LFB/HE) or Masson's Trichrome, respectively. The spinal cords for frozen sections were cryoprotected with 30% sucrose in 0.1 M phosphate buffer at 4°C and then frozen and embedded in frozen section medium compound (Stephens Scientific, Riverdale, NJ). Twenty-μm-thick parasagittal sections

FIG. 1. Surgical procedure for extramedullary chitosan channel implantation after spinal cord transection (**A and B**). At 14 weeks, gross appearance of the implanted channel (**C–H**) or spinal cord transection alone (**I and J**), from the dorsal and lateral aspects. In each panel, rostral is on the left. (**A**) Dorsal view of the transected spinal cord stumps placed within the transparent chitosan channel. The gap between the stumps is approximately 3.5 mm. (**B**) The spinal fusion with wire for spinal stabilization and the expanded polytetrafluoroethylene membrane placed on the dorsal aspect of the channel for prevention of scar invasion. (**C–H**) There is a tissue bridge inside the channels in the brain (**C and D**), spinal cord (**E and F**), and empty-channel groups (**G and H**). The brain group has the thickest bridge (**C and D**). In the no-channel group, there is pale connective tissue between the stumps (**I and J**). Color images available online at www.liebertpub.com/ten.

were cut in a 1:9 series on a cryostat and mounted on cold (–20°C) slides. The spinal cords for axon counts were preserved in universal fixative for 2 weeks. Segments of the cervical and upper thoracic spinal cord were sectioned transversely in a cryostat at 20 μm for BDA detection.

Immunohistochemistry

The following antibodies were used for the immunohistochemical assessments: mouse anti-neurofilament 200 monoclonal antibody (NF200); mouse anti-glial fibrillary acidic protein monoclonal antibody (GFAP); mouse anti-CC1/APC monoclonal antibody (CC1); mouse anti-microtube associated protein 2 monoclonal antibody (MAP2); mouse anti-rat nestin monoclonal antibody (nestin); mouse anti-3CB2 monoclonal immunoglobulin (Ig)M antibody (3CB2) to visualize radial glial cells; mouse anti-rat 192 IgG p75NTR monoclonal antibody (p75); mouse anti-rat prolyl 4-hydroxylase monoclonal antibody (rPH); rabbit anti-rat calcitonin gene–related peptide polyclonal antibody (CGRP); mouse anti-rat macrophage and monocyte monoclonal anti-

body (ED-1), and anti-rabbit type IV collagen polyclonal antibody (Col IV). The specificity, dilution, and source of each antibody is shown in Table 1. In all the immunohistochemistry procedures, appropriate negative controls were used with the omission of the primary antibodies.

Immunohistochemistry of frozen tissue and visualization of BDA. For immunohistochemistry in frozen sections, anti-NF200, GFAP, CC1, MAP2, nestin, 3CB2, p75, CGRP, rPH, and Col IV antibodies were used. The immunohistochemistry was performed as previously reported.[37–39] The sections were counterstained with the nuclear dye 4′,6-diamidino-2-phenylindole (DAPI) mounting medium (Vector Laboratories, Burlington, ON, Canada) and coverslipped. Every ninth slide in a series of frozen sections was selected for BDA detection. BDA procedure was performed as described previously.[17]

All sections were examined and photographed using a Zeiss-LSM 510 (Oberkochen, Germany) confocal microscope. Z-stack images were taken based on 20 to 40 optical sections at 0.5 μm in height per section. Then the entire thickness of the section was visualized using ImageJ soft-

TABLE 1. SPECIFICITY, DILUTION AND SOURCE OF THE ANTIBODIES

Antibody	Specificity	Dilution	Source
Antibodies for immunohistochemistry (Frozens)			
NF200	Neurons and axons	1:500	Sigma, Saint Louis, MS, U.S.A.
GFAP	Reactive astrocytes	1:200	Chemicon, Temecula, ON, Canada
CC1	Oligodendrocytes	1:1000	Calbiochem, San Diego, CA, U.S.A.
MAP2	Neurons and dendrites	1:500	Chemicon
nestin	Progenitor cells	1:100	BD Bioscience Pharmingen, Mississauga, ON, Canada
3CB2	Radial glial cells	1:50	Hybridoma Bank, University of Iowa, Iowa City, IA, U.S.A.
p75	Schwann cells	1:100	A gift from Dr. P. Baker, McGill University, Montreal, OB, Canada
rPH	Fibroblasts	1:100	Medicorp, Montreal, QB, Canada
CGRP	Sensory axons from DRG	1:3000	ImmunoStar, Hudson, WC, U.S.A.
ED-1	Activated macrophages	1:2000	Serotec, Raleigh, NC, U.S.A.
Co IV	Type IV collagen	1:50	Biodesign International, Saco, ME, U.S.A.
Antibodies for immunohistochemistry (Paraffins)			
NF200	See above	1:400	See above
ED-1	See above	1:200	See above

DRG; dorsal root ganglia.

ware system (National Institutes of Health, Bethesda, MD). Three-dimensional imaging was constructed using Imaris software (Bitplane, Exton, PA).

Immunohistochemistry of paraffin-fixed tissue. For immunohistochemistry of paraffin-embedded sections, anti-NF200 and ED-1 antibodies were used. The immunohistochemistry was performed as described previuosly.[17] The sections were observed under a Leica DMRB light microscope (Nussloch, Germany) and photographed using an image tiling and stitching system (Stereo Investigator Software, version 6, MicroBrightField, Inc, Williston, VT).

Stereological cell counts of GFP-positive cells

For stereological cell counts of GFP-positive cells in the brain and SC groups, the ninth equidistant frozen section from the spinal cord was selected from each animal and counterstained with DAPI. The spinal cords were observed using a Leica DMRB light microscope under 100× objective magnification, and the cell counts were performed using Stereo Investigator Software. The entire section of the spinal cord was divided by the sampling grid at 900 by 3000 μm, and the counting frame area was maintained at 30 by 30 μm and 15 μm in thickness. The average of 116.4 and 95.8 sampling grids per animal in the brain and SC groups, respectively, was determined. GFP-positive cells and their nuclei were observed under green and blue filters, respectively, and only GFP-positive cells containing DAPI-positive nuclei were counted as GFP-positive NSPCs. There was some autofluorescence in the spinal cord tissues after SCT visualized under a red filter, as previously reported,[40] and therefore, we also analyzed the GFP-positive cells containing DAPI-labeled nuclei under a red filter and found no GFP-positive cells containing DAPI-labeled nuclei.

Stereological analysis of differentiation of the NSPCs

To measure differentiation of the NSPCs in the brain and SC groups 14 weeks after channel implantation, five frozen spinal cord sections per rat containing the middle part of the tissue bridge in the channels were selected for each of the following histochemical reactions (anti-nestin, GFAP, CC1, MAP2, p75, and 3CB2 antibodies) and then counterstained with DAPI. Each immunostained-section was observed under a Leica DMRB light microscope with a 100× objective, and the cells were counted using Stereo Investigator Software. Each spinal cord section was equally divided by the sampling grid at 600 by 2000 μm, and the counting frame area was maintained at 30 by 30 μm and 15 μm in thickness. The average of 139 and 88.5 sampling grids per animal in the brain and SC groups, respectively, was counted. First, GFP-positive cells containing DAPI-labeled nuclei were counted under the green and blue filters as GFP-positive NSPCs. Second, these cells were observed under a red filter and counted as differentiated cells when they were also positive for each antibody. Then, the percentage of the differentiated NSPCs was calculated relative to the total number of GFP-positive NSPCs.

Transmission electron microscopy

One animal from each of the brain, SC, and empty-channel groups was randomly selected for transmission electron microscopy (TEM). Fourteen weeks after channel implantation, the animals were sacrificed using an intraperitoneal injection of sodium pentobarbital and transcardially perfused with 2% paraformaldehyde and 2.5% glutaraldehyde in 0.1 M sodium cacodylate buffer. The implanted channel was removed, and the tissue bridge was transected at the mid-point encompassing the narrowest part of the bridge. The tissue

inside the channel was postfixed in 1% osmium tetroxide. TEM sections were made as previously reported[41] and then viewed and photographed with a Hitachi H7000 transmission electron microscope (Tokyo, Japan).

Axon and blood vessel counts

The axon and blood vessel counts were performed on four animals from each of the brain, SC, and empty-channel groups. After removing the channels from the spinal cord tissues preserved in universal fixative, the 1-mm slice of the narrowest part of the tissue bridge was embedded in resin and then sectioned at 1-µm thickness. The 1-µm sections were stained with toluidine blue and viewed under a light microscope (Eclipse TE300, Nikon, Mississauga, Canada). Five sections per animal were randomly selected, and the following measurements were made: the area of the cross-sectional tissue bridge, the number of myelinated fibers,[14] and the number of blood vessels in each section without overlapping. With the help of Image Pro-Plus software (Media Cybernetics, Silver Spring, MD), the color-intensity-based method was used to identify and measure the following parameters of the myelinated fibers in high power fields:[37] the fiber diameter of the individual myelinated fibers, the thickness of the myelin, and the G-ratio (the ratio of the axon diameter to the entire fiber diameter). Histograms were generated with Sigma Plot 8.0 (Systat Software, Inc., Richmond, CA) for Windows.

Statistics

Data from the four groups were analyzed using one-way analysis of variance (ANOVA). The differences between two groups were analyzed using t-tests. Statistical analysis was performed using Sigma Plot 10 and Sigma Stat 3.5 for Windows.

RESULTS

Thick tissue bridge produced in the channel in brain group

At 14 weeks after channel implantation, gross observation under a surgical microscope showed no collapse or opacity of the channels. Through the transparent wall of the channels, tissue bridges were observed in the brain (Fig. 1C,D), SC- (Fig. 1E,F) and empty-channel groups (Fig. 1G,H). The brain group contained the thickest bridges, and in the no-channel group, the bridging tissue was thin, pale, and disorganized (Fig. 1I,J).

Numerous NSPCs survived in the tissue bridges and differentiated into mature glial cells in the brain group

LFB/HE-stained paraffin sections showed that the thick tissue bridges that formed in the channels in the brain group

consisted of two segments: a central portion that lay between the cord stumps and a lateral portion located on the sides of the central portion. The lateral portion extended rostro-caudally along the surfaces of the stumps within the channels (Fig. 2A, B). Fluorescent microscopy showed large numbers of GFP-positive cells in the central and lateral portions of the bridges (Fig. 2C). Stereological cell counts showed $3.3 \pm 2.0 \times 10^6$ GFP-positive cells in the bridges in the brain group (Fig. 5). Immunohistochemistry showed that some GFP-positive cells co-localized with GFAP-positive astrocytes (Fig. 2D–F) or CC1-positive oligodendrocytes (Fig. 2G–I). There were also many 3CB2-positive radial glial cells in the central portions of the bridges, but only a small number of GFP-positive cells showed co-localization with this antibody (Fig. 2J–L). Some GFP-positive cells co-localized with nestin-positive undifferentiated NSPCs (Fig. 2M–O). There were many NF200-positive axons in the central portions of the bridges, and GFP-positive cells were linearly related to these axons, but they did not co-localize with GFP-positive cells (Fig. 3A–C). With 3D imaging, many GFP-positive cells were seen to be closely associated with these NF200 positive axons (Fig. 3D). Many CGRP-positive sensory axons were also found in the bridge in relation to GFP-positive cells (Fig. 3E). There were some p75-positive Schwann cells in the central bridge (Fig. 3F) and many rPH-positive fibroblasts in the central and lateral bridges (Fig. 3G). However, double-label immunohisto-chemistry showed no co-localization of either of these cells with GFP-positive cells (Fig. 3F,G). There were no MAP-2 positive neurons in the bridges. Stereological analysis showed that 24.8, 17.4, 3.39 or 10.0% of the GFP-positive cells in the brain group colocalized with anti-GFAP, CC1, 3CB2 or nestin antibody, respectively (Table 2). Interestingly, there was some Col IV in the central portion of the bridges, but there was no Col IV in the lateral portion of the bridges (Fig. 3H). ED-1 immunostained sections showed a massive aggregation of macrophages in the white matter of the stumps and a small number of macrophages in the central portion of the bridges, but there were almost no macrophages in the lateral portions of the bridges (Fig. 3I).

There were a small number of GFP-positive cells in the white and gray matter of the stumps located in the channels, indicating migration of the GFP-positive cells from the tissue bridge into the spinal cord stumps. However, there was no evidence for migration of GFP-positive cells into the host spinal cord beyond the channels.

TEM revealed that in the central portions of the bridges there were many axons myelinated by Schwann cells, but not by oligodendrocytes, and there were also some fibroblasts identified by their endoplasmic reticulum and by their production of collagen. There was a large amount of collagen in the central and lateral portions of the bridges revealed by Masson's Trichrome stain and TEM. The corticospinal tract rostral to the transection site was well labeled with BDA, but there were no BDA-labeled fibers in the bridges or in the caudal spinal cord.
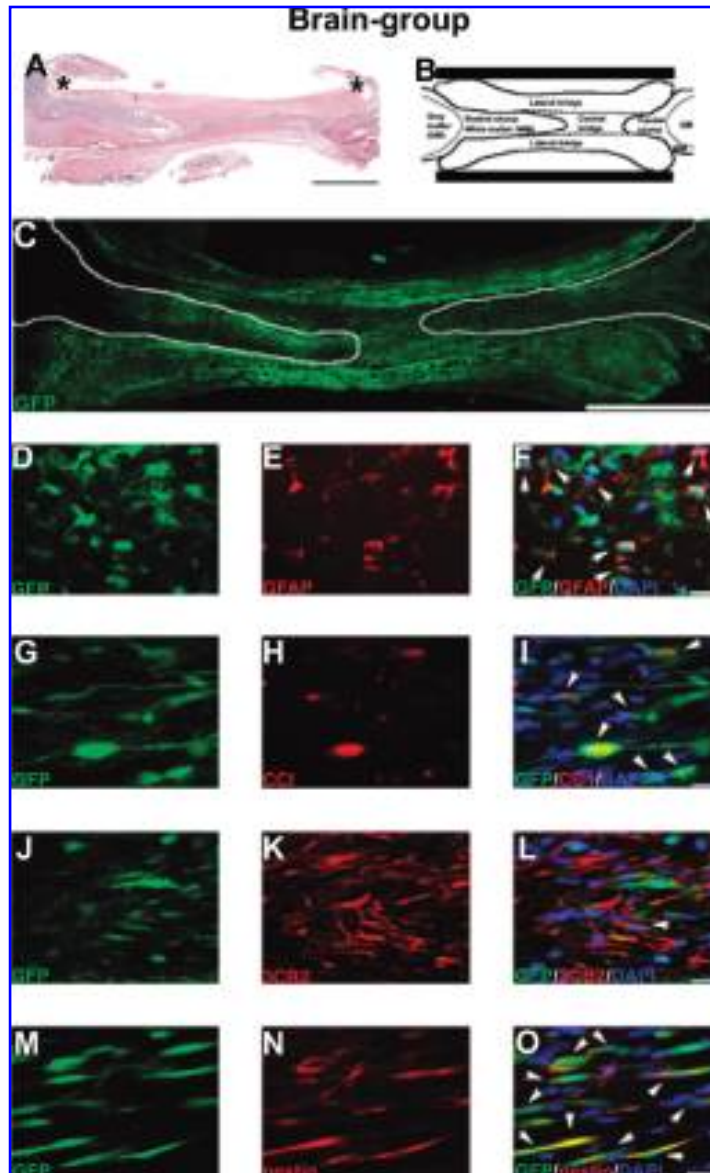
FIG. 2. (**A**) Twenty-μm parasagittal Luxol Fast Blue and hematoxylin and eosin–stained paraffin section. (**B**) A schematic drawing of the tissue bridge inside channel. (**C**) Twenty-μm parasagittal frozen section. (**D–O**) Confocal photomicrographs of 20 μ parasagittal frozen sections 14 weeks after channel implantation in the brain group. In each panel, rostral is on the left. The channel walls were removed before sectioning, and therefore, there are some spaces corresponding to the remnants of the rostral and caudal ends of the channel (asterisks in **A**). The sections of the entire tissue bridge (**A and C**) were obtained using an image tiling and stitching system (Stereo Investigator Software version 6). The entire tissue bridge in **C** was obtained using the following procedure. First, a non-immunostained section of the bridge was photographed under a green or red filter. Some autofluorescence and macrophages in the tissue bridge were detected under a red filter. Second, these photographs were merged using Adobe Photoshop 7.0. Then, the yellow color in the merged photograph, corresponding to the autofluorescence and macrophages, was converted to black. Thus, the green signal corresponds exclusively to green fluorescent protein (GFP)-positive cells (**C**). Confocal laser scanning Z-stack images were composed of 20 to 40 confocal laser scanning micrographs at 0.5 μm in height per section in the bridges (**D–O**). GFP signal is in green (**C, D, F, G, I, J, L, M and O**). Glial fibrillary acidic protein (GFAP), mouse anti-CC1/APC monoclonal antibody (CC1), mouse anti-3CB2 monoclonal immunoglobulin (Ig)M antibody (3CB2), or nestin-signal is in red (**E and F** for GFAP, **H and I** for CC1, **K and L** for 3CB2 and **N and O** for nestin, respectively), and 4′,6-diamidino-2-phenylindole signal is in blue (**F, I, L and O**). Co-localized signals with green or red and blue are in yellow and azure, respectively (**F, I, L and O**). (**A**) There is a thick eosinophilic tissue bridge in the channel in the brain group. (**B**) Scheme of the tissue bridge in the channel showing the central and lateral portions of the bridge. (**C**) There are a large number of GFP-positive cells in the tissue bridge. The outline of the rostral and caudal stumps is drawn in **C**. (**D–F and G–I**) Some GFP-positive cells overlap with GFAP (**D–F**) and CC1-positive cells (**G–I**) corresponding to astrocytes and oligodendrocytes, respectively. (**J–L**) A few GFP-positive cells overlap with 3CB2-positive cells corresponding to radial glial cells. (**M–O**) Some GFP-positive cells overlap with nestin-positive cells corresponding to undifferentiated cells. Scale bars in **A** and **C** = 2 mm; **F, I, L** and **O** = 20 μm Color images available online at www.liebertpub.com/ten.
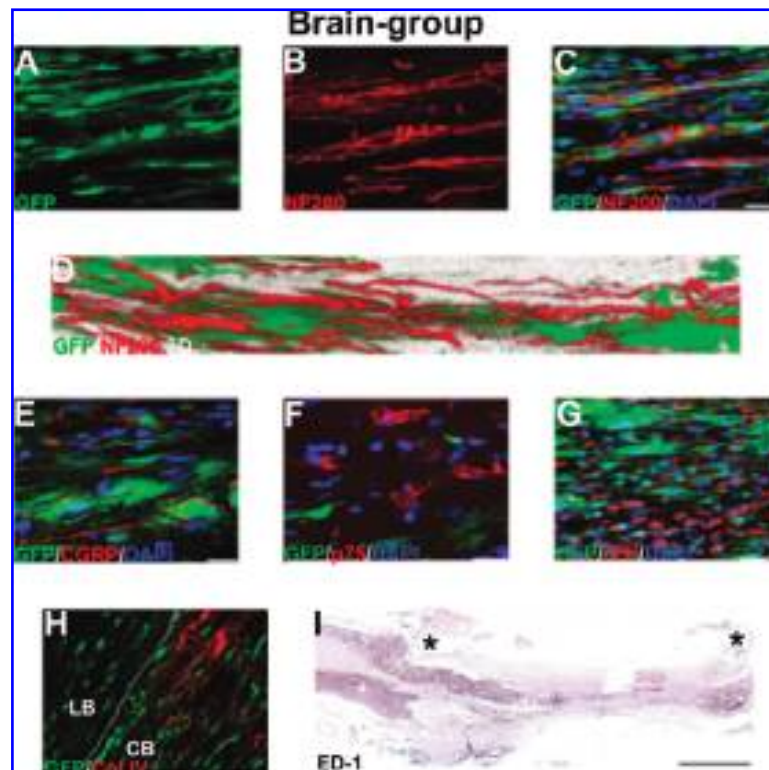
FIG. 3. Z-stack images of 20 to 40 confocal laser scanning micrographs per parasagittal frozen section of the tissue bridge (**A–H**) and 20-μm parasagittal paraffin section immunostained with anti-ED1 antibody for macrophages (**I**) 14 weeks after channel implantation in the brain group. Three-dimensional image reconstructed for a merged image of the tissue bridge shown in **C** using Imaris software (**D**). Confocal laser scanning Z-stack images (**A–C, E–H**). Green fluorescent protein (GFP) signal is in green (**A, C–H**). Mouse anti-neurofilament 200 monoclonal antibody (NF200), rabbit anti-rat calcitonin gene–related peptide polyclonal antibody (CGRP), mouse anti-rat 192 IgG p75NTR monoclonal antibody (p75), mouse anti-rat prolyl 4-hydroxylase monoclonal antibody (rPH), and collagen (Col) IV signals are in red (**B–D** for NF200, **E** for CGRP, **F** for p75, **G** for rPH, and **H** for Col IV), and 4′,6-diamidino-2-phenylindole signal is in blue (**C, E–G**). Co-localized signals with green or red and blue are in yellow and azure, respectively (**C, E–G**). (**A–C**) GFP-positive cells in the central tissue bridge are linearly aligned to NF200-positive axons, but they do not overlap. (**D**) Three-dimensional image demonstrates that the GFP-positive cells are in contact with NF200-positive axons. (**E**) CGRP-positive axons corresponding to sensory axons are observed in the bridge in relation to GFP-positive cells. (**F and G**) There is no co-localization of p75- (for Schwann cells), rPH-positive (for fibroblasts) cells (**F**), or fibroblasts with GFP-positive cells in the bridge. (**H**) There is some Col IV in the central portion (CB in **H**) but not in the lateral portion of the bridge (LB in **H**). (**I**) Mouse anti-rat macrophage and monocyte monoclonal antibody immunostaining shows a massive aggregation of macrophages in the white matter of the stumps and a small number in the central portion of the bridge but not in the lateral portion of the bridge. Asterisks show the location of the ends of the channel walls. Scale bars in **C, E and F** = 20 μm; **G and H** = 50 μm, **I** = 2 mm. Color images available online at www.liebertpub.com/ten.

Fewer NSPCs survived in the tissue bridges in the SC group than in the brain group

At 14 weeks after channel implantation, LFB/HE stained paraffin sections from the SC group showed tissue bridges which were thinner than those in the brain group (Fig. 4A). There was also a large amount of collagen in these bridges shown by Masson's Trichrome staining (Fig. 4B). Fluorescent microscopy showed many GFP-positive cells in the bridge, but less than in the brain group (Fig. 4C), and stereological cell counts showed that there were $6.6 \pm 4.1 \times 10^5$ GFP-positive cells in the bridges in the SC group, significantly less than in the brain group ($P = 0.027$) (Fig. 5). Double label immunohistochemistry showed that some GFP-

positive cells colocalized with GFAP-positive astrocytes (Fig. 4D–F), CC1-positive oligodendrocytes (Fig. 4G–I) and nestin-positive undifferentiated NSPCs (Fig. 4J–L). Also, there were many 3CB2-positive radial glial cells, some p75-positive Schwann cells, and a large number of rPH-positive fibroblasts in the bridges, and none of the latter colocalized with GFP-positive cells as expected. GFP-positive cells were linearly related to NF200-positive axons in the central portions of the bridges, but the cells were not colocalized with those axons, similar to the pattern observed in the brain group (Fig. 4M–O). There were some CGRP-positive sensory axons but no MAP2-positive cells in the tissue bridges. Stereological analysis showed that 31.3%, 9.7%, and 34.4% of the GFP-positive cells in SC group co-localized with anti-

Table 2. Differentiation of the Adult Rat Brain- or Spinal Cord Derived NSPCs in the Chitosan Channels

	GFAP (%)	CC1 (%)	3CB2 (%)	MAP2 (%)	p75 (%)	rPH (%)	Nestin (%)
Brain-group	24.8	17.4	3.39	0	0	0	10.0
SC-group	31.8	9.7	0	0	0	0	34.4

GFAP, CC1, and nestin antibody, respectively (Table 2). TEM revealed that there were many axons myelinated by Schwann cells in the central portion of the bridges (Fig. 6A, B), as well as fibroblasts producing collagen. There was no Col IV in the bridge, and there were no BDA-labeled fibers in the bridge and caudal spinal cord.

Tissue bridges contained myelinated axons in the empty-channel group and connective tissue only in the no-channel group

At 14 weeks after channel implantation, LFB/HE-stained sections in the empty-channel group showed a narrow tissue bridge in the channel (Fig. 7A) composed of connective tissue. There were some NF200-positive axons in the bridge (Fig. 7B), and TEM showed that the bridges contained many axons myelinated by Schwann cells (Fig. 6C.D) and unmyelinated axons (Fig. 6E). There were also fibroblasts producing collagen (Fig. 6D,F). There were no BDA-labeled fibers in the bridge and caudal spinal cord.

In the no-channel group 14 weeks after SCT, there was a narrow connective tissue bridge between the stumps of the spinal cord (Fig. 7C). Masson's Trichrome–stained section revealed that there was a thick collagen layer between the stumps, often oriented perpendicular to the long axis of the spinal cord (Fig. 7D). There were no BDA-labeled fibers in this connective tissue or in the caudal spinal cord.

Myelinated fibers and blood vessels were apparent in the tissue bridges in the brain, SC, and empty-channel groups

One-μm cross-sections revealed myelinated fibers and blood vessels concentrated in the central portion of the bridges, but there were no myelinated fibers in the lateral portion of the bridges in the brain (Fig. 8A–C), SC (Fig. 8D, E), or empty-channel groups (Fig. 8F) 14 weeks after channel implantation. The cross-sectional areas of the bridges in the brain, SC, and empty-channel groups were $1.82 \pm 0.61 \, mm^2$, $0.73 \pm 0.41 \, mm^2$, and $0.40 \pm 0.32 \, mm^2$, respectively, and there were significant difference between the brain group and the SC and empty-channel groups ($p < 0.001$) (Fig. 8G). The total number of myelinated fibers in the brain, SC, and empty-channel groups was 429 ± 198, 498 ± 512, and 666 ± 370, respectively, but there was no significant difference between the groups ($p = 0.14$) (Fig. 8H). There was an average of only 12 fibers in the no-

channel group. The total number of blood vessels in the brain, SC, and empty-channel groups was 134 ± 24, 150 ± 81, and 128 ± 67, respectively, and there was no significant difference between the groups ($p = 0.92$) (Fig. 8I). Also, there was no significant difference between the groups in fiber diameter (Fig. 8J), myelin thickness (Fig. 8K), or G-Ratio (Fig. 8L) ($p = 0.88$, $p = 0.51$, $p = 0.42$, respectively), suggesting that the myelinated fibers in the three groups were morphologically similar.

Functional evaluation

There was no significant difference in BBB scores at 12 weeks between the brain, SC, empty-channel, and no-channel groups (one-way ANOVA, $p = 0.95$) (Fig. 9). No animal achieved plantar placement of the paw with weight support (corresponding to a BBB score of 9).

DISCUSSION

This is the first report of the implantation of extra-medullary chitosan channels seeded with NSPCs derived from the adult rat brain or spinal cord after complete SCT, the most severe form of experimental SCI. The combination of NSPCs and channels was successful with respect to the survival of large numbers of the cells that differentiated into mature astrocytes and oligodendrocytes. Of the brain, SC, and empty-channel groups, the brain group had the thickest bridge containing the largest number of surviving NSPCs at 14 weeks after transplantation. The SC group had tissue bridges that were significantly smaller and contained approximately one-fifth the number of NSPCs as the brain group. The empty-channel group also showed tissue bridges, but they were composed mainly of fibroblasts synthesizing collagen, findings similar to those reported by Spilker et al.[42] in a study of collagen conduits in SCT. In our study, there was more collagen in the brain–NSPC group than in the empty-channel group. The collagen matrix synthesized by the fibroblasts may have acted as a suitable biological scaffold and assisted the long-term survival of the brain-derived NSPCs.

In our previous review of bioengineered strategies for spinal cord repair,[2] we noted several promising reports of the combination of synthesized scaffolds or channels and transplanted cells including Schwann cells,[43] olfactory ensheathing cells,[44] and NSPCs.[8,45,46] With respect to NSPCs for repair of SCI, Teng et al.[8] reported that implantation of a poly(lactic-coglycolic acid)-based scaffold seeded with mouse-embryonic NSPCs showed significant functional motor recovery in a spinal cord hemisection model in the rat. They found axonal regeneration from the sensorimotor cortex, but the transplanted NSPCs showed no differentiation into mature neural cells and were double-labeled only with anti-nestin antibody 10 weeks after transplantation.[8] In contrast, we showed a significant differentiation of transplanted
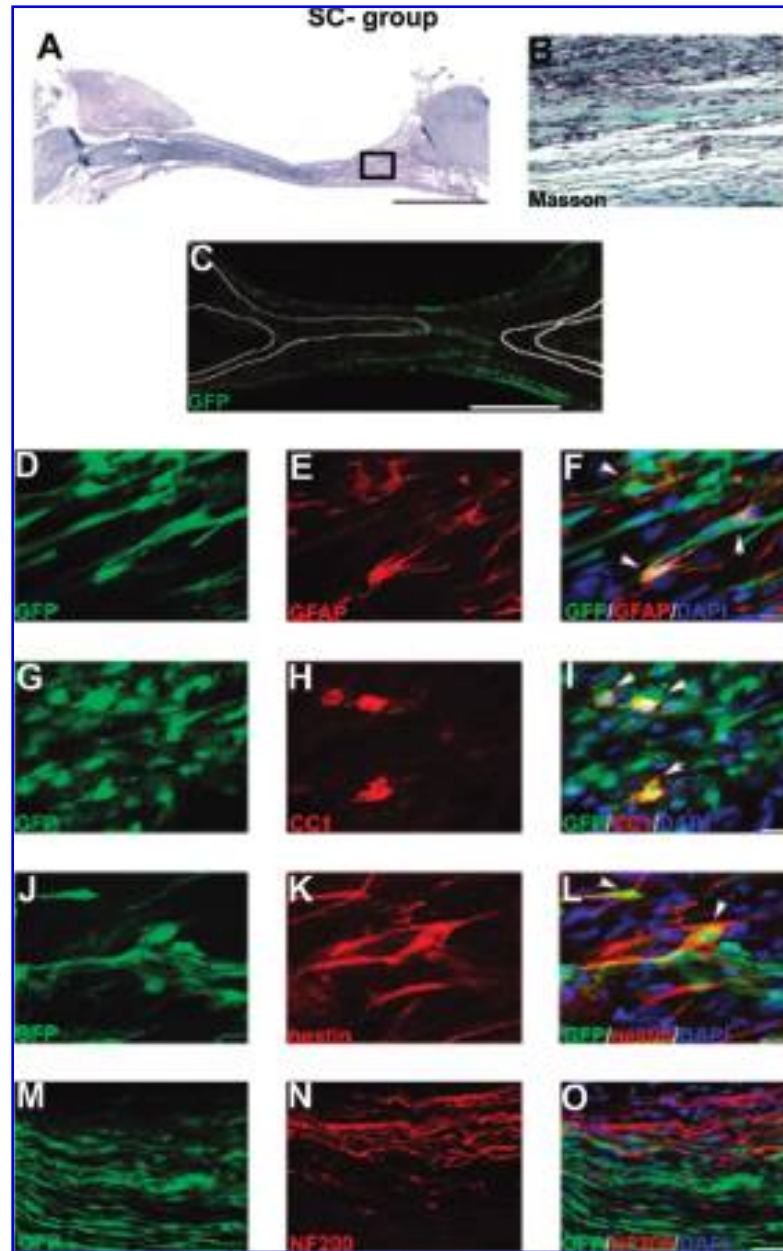
FIG. 4. Twenty-μm parasagittal Luxol Fast Blue and hematoxylin and eosin (LFB/HE)- (**A**) and Masson's Trichrome-stained (**B**) paraffin section, 20-μm parasagittal frozen section, (**C**) and confocal photomicrographs of 20-μm parasagittal frozen sections (**D–O**) 14 weeks after channel implantation in the spinal cord. The sections of the entire tissue bridge were obtained using an image tiling and stitching system (Stereo Investigator Software version 6) (**A and C**). The entire tissue bridge in the frozen section in **C** was obtained with the same procedure as in Figure 2C. Confocal laser scanning Z-stack images were composed of 20 to 40 confocal laser scanning micrographs per section of the bridges (**D–O**). Green fluorescent protein (GFP) signal is in green (**C, D, F, G, I, J, L, M and O**). Glial fibrillary acidic protein (GFAP), mouse anti-CC1/APC monoclonal antibody (CC1), nestin, and mouse anti-neurofilament 200 monoclonal antibody (NF200) signals are in red (**E and F** for GFAP, **H and I** for CC1, **K and L** for nestin, and **N and O** for NF200), and 4′,6-diamidino-2-phenylindole signal is in blue (**F, I, L and O**). Co-localized signals with green or red and blue are in yellow and azure, respectively (**F, I, L and O**). (**A**) LFB/HE-stained section shows a tissue bridge inside the channel, which is smaller than in the brain group in Figure 2A. (**B**) Masson's Trichrome–stained section corresponding to the boxed area in **A** shows a large amount of collagen in blue in the bridge. (**C**) There are many GFP-positive cells in the bridge. The outlines of the white and grey matter of the stumps are drawn in **C**. (**D–F, G–I and J–L**) Some GFP-positive cells overlap with GFAP-positive cells (**D–F**), CC1-positive cells (**G–I**), and nestin (**J–L**), corresponding to astrocytes, oligodendrocytes, and undifferentiated neural stem and progenitor cells, respectively. (**M–O**) GFP-positive cells in the tissue bridge are linearly aligned to NF200-positive axons, but they are not overlapped. Scale Bars in **A** = 2 mm, **B** = 100 μm, in **C** = 1 mm, **F, I and L** = 20 μm, and **O** = 50 μm. Color images available online at www.liebertpub.com/ten.
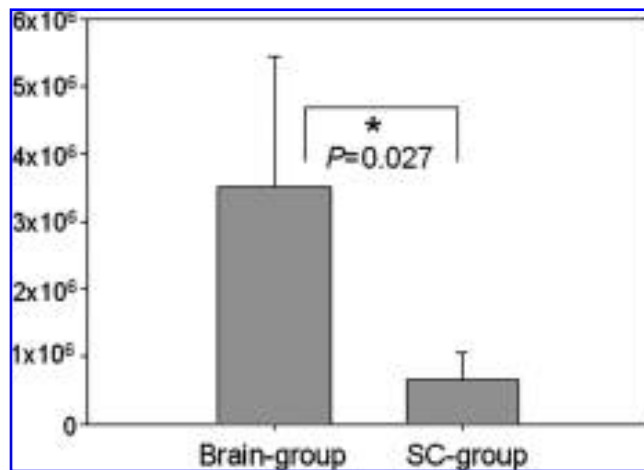
FIG. 5. Histogram showing the stereological cell counts of the neural stem and progenitor cells (NSPCs) in the tissue bridges 14 weeks after channel implantation in the brain and spinal cord (SC) groups. The Y-axis of the histogram indicates the number of NSPCs in the tissue bridges. There were $3,312,000 \pm 2,031,000$ and $657,000 \pm 409,000$ NSPCs in the bridges in the brain and SC groups, respectively, and the difference was significant ($p = 0.03$).

There have been several studies showing good biocompatibility between chitosan channels and injured peripheral nerves,[48–51] and recently we implanted chitosan channels containing peripheral nerves into the cavitated injury site after severe clip-compression SCI and found thick bridges containing numerous regenerating myelinated axons in the channels (unpublished data). In the present study, chitosan channels also demonstrated excellent biocompatibility with the transplanted NSPCs and the injured spinal cord. There was minimal accumulation of macrophages inside the channels with brain- or SC-derived NSPCs. There was a much lower incidence of caudal migration of the rostral stump and syringomyelia than we reported previously with other hydrogel channels.[17] These properties make chitosan an attractive biomaterial for combination therapy involving cell transplantation.

In the present study, the adult brain–derived NSPCs differentiated into mature astrocytes (24.8%) and oligodendrocytes (17.3%) but not neurons, whereas 10% were nondifferentiated cells showing nestin-immunoreactivity (Table 2). Recently, our group reported that brain-derived NSPCs cultured on laminin-coated tissue culture slides for 7 days differentiated into neurons ($10.7 \pm 2.9\%$), astrocytes ($12.6 \pm 3.6\%$), and oligodendrocytes ($40.6 \pm 4.4\%$), and many cells were nestin-positive ($23.1 \pm 3.4\%$). In addition, NSPCs cultured on chitosan matrices for 48 h differentiated into astrocytes ($4.4 \pm 1.9\%$), oligodendrocytes ($5.5 \pm 2.3\%$), and a small number of neurons ($1.4 \pm 1.04\%$) *in vitro*. However, when the NSPCs seeded on chitosan channels were implanted after SCT, there was differentiation at 5 weeks into astrocytes ($9.9 \pm 1.2\%$), oligodendrocytes ($23.2 \pm 6\%$), and nestin-positive cells ($18.3 \pm 3.6\%$),

cells in the brain and SC groups. The functional recovery noted by Teng *et al.* might have been due to the secretion of neurotrophic factors by the transplanted NSPCs as suggested by the study of Lu *et al.*[47] or to the use of the hemisection model, in which intact tissue also provides these factors. Although Teng's study showed great potential for this bioengineered strategy with NSPCs, there have been no confirmatory studies reported.

FIG. 6. Transmission electron microscopy of the central tissue bridges 14 weeks after channel implantation in the spinal cord (SC) (**A and B**) and empty-channel (**C–F**) groups. (**A**) There are several myelinated fibers (arrowheads) in the central portion of the tissue bridge in the SC group. One myelinated fiber (star) is contained in one Schwann cell (asterisk). (**B**) A myelinated fiber is surrounded by a basal lamina, which is characteristic of the Schwann cell (arrow in **B**). (**C**) There are many Schwann cells with basal lamina (box in **C**) associated with myelinated fibers in the central portion of the bridge in the empty-channel group. (**D**) There is fibroblast-producing collagen in the endoplasmic reticulum (star) and myelinated fibers in the central bridge. (**E**) There are many non-myelinated fibers (arrowheads) contained in one Schwann cell in the central portion of the bridge. (**F**) There are a number of fibroblasts associated with a large amount of collagen in the lateral portion of the bridge. Bars in **A, C, D and F** = 1 μm; **B** = 0.2 μm, **E** = 0.5 μm.
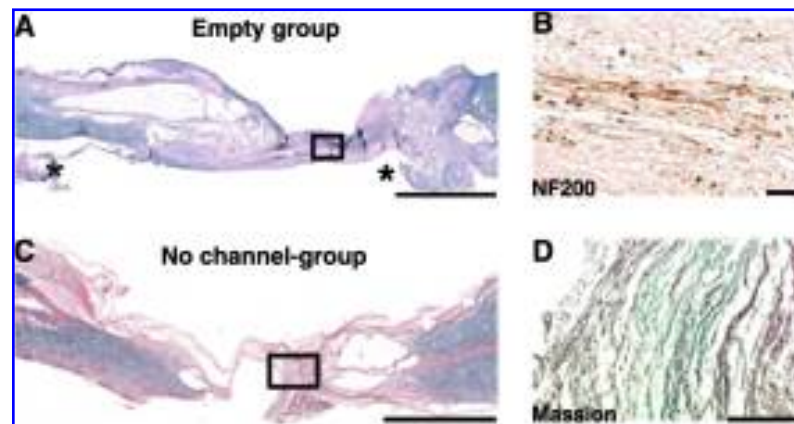
FIG. 7. Twenty-μm parasagittal paraffin section stained with Luxol Fast Blue and hematoxylin and eosin (LFB/HE) (**A**) and immunostained with anti-mouse anti-neurofilament 200 monoclonal antibody (NF200) antibody (**B**) 14 weeks after channel implantation in the empty-channel group and 20-μm parasagittal LFB/HE- (**C**) and Masson's Trichrome-stained (**D**) paraffin section 14 weeks after spinal cord transection in the no-channel group. (**A**) A LFB/HE-stained section shows that there has been caudal migration of the rostral stump and the development of multiple syringomyelic cavities in this stump. The asterisks in **A** indicate the location of the ends of the channel. (**B**) NF200-immunostained section of an adjacent section corresponding to the boxed area in **A**. There are some NF200-positive axons in the central portion of the tissue bridge. (**C**) LFB/HE-stained section showing fibrous connective tissue between the stumps. (**D**) The boxed area in **C** in an adjacent section stained with Masson's Trichrome reveals a thick collagen layer in a vertical direction in the fibrous tissues between the stumps. Bars in **A and C** = 2 mm, **B** = 50 μm, **K** = 200 μm. Color images available online at www.liebertpub.com/ten.

but no neurons were generated, similar to the present study.[25] In contrast, the *in vitro* differentiation studies with brain-derived NSPCs on chitosan in the presence of serum and absence of mitogens indicated that these cells can give rise to all three neuronal phenotypes (unpublished data). These findings suggest that environmental factors within the damaged spinal cord influence the *in vivo* differentiation of NSPCs. The comparison of the previous 5-week data and the present 14-week data suggests that longer-term survival may favor astrocytes over oligodendrocytes. This phenomenon may relate to the observation that astrocytes are the prominent cell type produced from endogenous neural stem cells in the region of the central canal after SCI.[27] Another possible explanation is that oligodendrocytes may not survive for the duration of the 5 weeks *in vivo* in the injured cord. Our results are also consistent with the possibility that the injured spinal cord inhibits differentiation of NSPCs into mature neurons.

The adult spinal cord–derived NSPCs differentiated into a higher percentage of mature astrocytes (31.8%) and a lower percentage of mature oligodendrocytes (9.7%) and no neurons, whereas 31.8% of the cells were nestin-positive. Thus, there were differences in differentiation between brain- and spinal cord–derived NSPCs from the same adult GFP rats, and there were still a large number of nestin-positive cells after 14 weeks in the SC group. In terms of *in vitro* differentiation of the spinal cord–derived NSPCs, we previously reported 18%, 58%, and 7.4% of the NSPCs prepared using identical methods differentiated into astrocytes, oligodendrocytes, and neurons, respectively, *in vitro*.[34] Also, adult rat spinal cord–derived NSPCs transplanted into the normal and partially injured spinal cord differentiated into large num-

bers of oligodendrocytes and astrocytes but no neurons.[37,38] These data suggest that not only the origin of the NSPCs, but also the environment of the transplanted cells, affect differentiation of NSPCs, as previously reported.[52,53] For example, it is known that signals from fibroblasts induce adult intestinal epithelial cells to form more-primitive embryonic nestin-positive cells.[54] The fibroblasts that migrated into the chitosan channels in the present study may have influenced the differentiation of the NSPCs.

After transplantation of brain-derived NSPCs in the present study, 3.4% of the NSPCs were immunopositive for 3CB2, indicating differentiation into radial glial cells. Radial glia are known to facilitate cell migration and axon growth in the developing CNS but also appear to be the precursors of astrocytes,[55] macrophages and microglia,[56] and neurons.[57] In contrast, we did not find any NSPCs differentiating into radial glial cells in the SC group.

In the brain and SC groups, a small proportion of the NSPCs migrated a short distance into the adjacent host spinal cord, although the migration did not extend beyond the length of the channels. It is possible that the large aggregation of macrophages in the stumps provided a hostile environment to the NSPCs, preventing further migration.

Collagen is the most abundant extracellular matrix protein and plays a dominant role in maintaining the structural integrity of various tissues.[58,59] At least 27 types of collagen with 42 distinct polypeptide chains have been identified.[60,61] Among them are collagen types that form fibrils (types I-III, V, XI, XXIV, and XXVII) synthesized by fibroblasts or chondrocytes. In contrast, collagen type IV forms beaded filaments and is contained in basal membranes and synthesized by endothelial cells, astrocytes, meningeal fibroblasts,
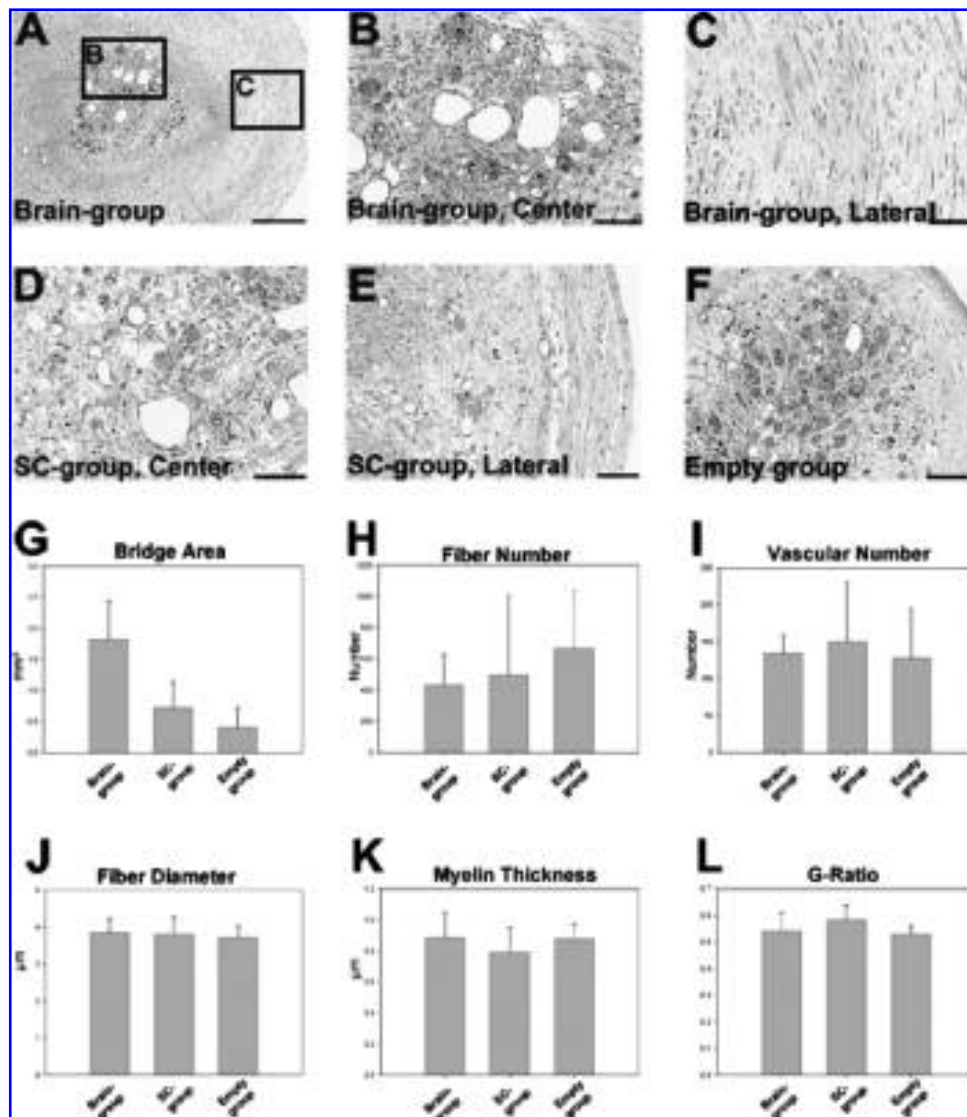
FIG. 8. (**A–F**) One-μm cross-sections 14 weeks after channel implantation in brain (**A–C**), spinal cord (SC) (**D and E**), and empty-channel (**F**) groups. (**G–L**) Histograms showing bridge area (**G**), fiber number (**H**), vessel number (**I**), fiber diameter (**J**), myelin thickness (**K**), and G-ratio (**L**) in brain, SC, and empty-channel groups. (**A–C**) The boxed areas in **A** are magnified in **B** and **C**. The brain group shows many myelinated axons and blood vessels in the central portion of the bridge (**A and B**) and no myelinated axons in the lateral portion of the bridge (**A and C**). There are many myelinated axons and blood vessels in the central portion of the bridge (**D**) but no axons in the lateral portion of the bridge in the SC group (**E**). In the empty-channel group, there are many myelinated axons and blood vessels in the central portion of the bridge (**D**) but no axons in the lateral portion of the bridge (**F**). (**G**) Area of the cross-sections of the bridges in brain, SC, and empty-channel groups is 1.82 ± 0.61, 0.73 ± 0.41, and $0.40 \pm 0.32\,\mathrm{mm}^2$, respectively, and there was a significant difference between the brain group and the SC and empty-channel groups ($p < 0.001$). (**H**) The total number of myelinated fibers in the brain, SC, and empty-channel groups was 429 ± 198, 498 ± 512, and 666 ± 370, respectively, and there was no significant difference between the groups ($p = 0.144$). The corresponding number in the no-channel group was 12 ± 10. (**I**) The total number of blood vessels in the brain, SC, and empty-channel groups was 134 ± 24, 150 ± 81, and 128 ± 67, respectively, and there was no significant difference between the groups ($p = 0.92$). (**J–L**) There was no significant difference between all the groups in fiber diameter (**J**), myelin thickness (**K**), or G-Ratio (**L**) ($p = 0.88$, 0.51, and 0.42, respectively).

or Schwann cells.[62–65] Fibrous tissue scarring in response to SCI acts as an impediment to axonal regrowth, and collagen is one of the major components of the lesion scar.[66] In particular, type IV collagen is known to be a key matrix in dense fibrous scar formation in the acute phase of SCI and causes failure of spontaneous axonal regeneration.[67,68] Suppression of fibrous scarring by type IV collagen resulted in long axonal regeneration.[65] In contrast, bridging the defect in the spinal cord after complete SCT with type I collagen filaments contributed to formation of a firm tissue cable containing
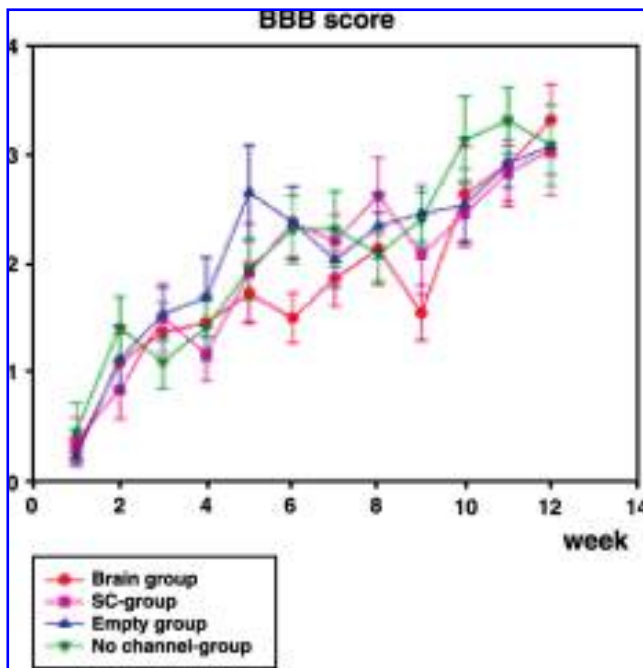
FIG. 9. Functional evaluation using Basso, Beattie, Bresnahan (BBB) scoring in brain, spinal cord, empty-channel, and no-channel groups for 12 weeks after channel implantation. There was no significant difference in the BBB scores at 12 weeks between the four groups (one-way analysis of variance, $p = 0.95$). Bar = mean ± standard error. Color images available online at www.liebertpub.com/ten.

numerous myelinated regenerating axons and achieved significant functional recovery.[69,70] Moreover, a combination of type I collagen solution and neonatal astrocytes implanted into the cavity after spinal cord hemisection promoted axonal regeneration.[71] In the present study, there was a large amount of type I–like fibular collagen likely synthesized by fibroblasts more in the lateral portions of the bridges and less in the central portions of the bridges. In contrast, based on immunohistochemistry with anti-type IV collagen antibody, we found that type IV collagen was located only in the central portion of the bridges. Considering the co-localization of Schwann cells and blood vessels in the central bridges, it is likely that the type IV collagen is a component of the basal membrane synthesized by Schwann cells or formed by the endothelial cells of blood vessels. Although there were a number of GFAP-positive NSPCs that differentiated into astrocytes in the lateral portions of the bridges, there was no association with type IV collagen in the lateral portion of the bridges, although there was type IV collagen in the central portion in the brain and SC groups. Thus, it is unlikely that NSPCs synthesize type IV collagen. In the channel implantation groups, collagen fibers inside the channels were arranged in a linear direction parallel to the channels and may have played a role in axonal guidance in the central portions of the bridges. In contrast, in the no-channel group, there was often a thick collagen layer perpendicular to the long axis of

the stumps, which may have blocked regenerating axons, as others have also reported.[42]

Despite the firm tissue bridge containing many surviving and differentiated NSPCs, neither the brain- nor SC-derived cells and channels increased the axonal regeneration or functional recovery. Perhaps this is related to the restriction of the regenerating axons and blood vessels to the central portion of the bridges extending directly between the stumps of the host spinal cord. It appears that axons entering the lateral portions of the bridge may not have been able to penetrate into the spinal cord stumps and therefore would be nonfunctioning conduits. In the central portions of the bridges, the NSPCs were spatially aligned with the NF200-positive axons. However, there was no definite evidence that the NSPCs contributed to the myelination observed using electron microscopy. We found axons myelinated by Schwann cells in the bridges, indicating that Schwann cells that had migrated from adjacent nerve roots performed at least some of the axonal myelination in the bridges. In the channel groups, the bridges contained some CGRP-positive sensory axons, but there were no BDA-positive axons from the corticospinal tract.

To improve functional recovery with NSPC-containing channels, additional factors can be added, such as anti-Nogo-A[72] to enhance supraspinal axonal regeneration, or neurotrophic factors, to influence NSPC differentiation. The channels may be particularly well suited for local release of a high concentration of these agents at the injury site.

CONCLUSION

Implantation of extramedullary chitosan channels in combination with transplantation of NSPCs successfully achieved long-term survival of adult rat brain– and SC-derived NSPCs after SCT in rats. The number of surviving NSPCs in the brain group was approximately five times as great as in the SC group, and the brain group produced the thickest bridges. In both groups, the tissue bridges contained abundant collagen. At 14 weeks, brain- and SC-derived NSPCs seeded in the channels differentiated into oligodendrocytes and astrocytes, with some cells remaining as neural progenitors. Although chitosan channel implantation created tissue bridges containing many axons after SCT, there was no improvement in functional recovery.

ACKNOWLEDGMENTS

REFERENCES

1. Kulbatski, I., Mothe, A.J., Nomura, H., and Tator, C.H. Endogenous and exogenous CNS derived stem/progenitor cell approaches for neurotrauma. Curr Drug Targets **6,** 111, 2005.

2. Nomura, H., Tator, C.H., and Shoichet, M.S. Bioengineered strategies for spinal cord repair. J Neurotrauma **23,** 496, 2006.

3. Tator, C.H. Review of treatment trials in human spinal cord injury: issues, difficulties, and recommendations. Neurosurgery **59,** 957, 2006.

4. Schumm, M.A., Castellanos, D.A., Frydel, B.R., and Sagen, J. Improved neural progenitor cell survival when cografted with chromaffin cells in the rat striatum. Exp Neurol **185,** 133, 2004.

5. Enzmann, G.U., Benton, R.L., Talbott, J.F., Cao, Q., and Whittemore, S.R. Functional considerations of stem cell transplantation therapy for spinal cord repair. J Neurotrauma **23,** 479, 2006.

6. Vroemen, M., Aigner, L., Winkler, J., and Weidner, N. Adult neural progenitor cell grafts survive after acute spinal cord injury and integrate along axonal pathways. Eur J Neurosci **18,** 743, 2003.

7. Kwon, Y.K. Effect of neurotrophic factors on neuronal stem cell death. J Biochem Mol Biol **35,** 87, 2002.

8. Teng, Y.D., Lavik, E.B., Qu, X., Park, K.I., Ourednik, J., Zurakowski, D., Langer, R., and Snyder, E.Y. Functional recovery following traumatic spinal cord injury mediated by a unique polymer scaffold seeded with neural stem cells. Proc Natl Acad Sci U S A **99,** 3024, 2002.

9. Willerth, S.M., Arendas, K.J., Gottlieb, D.I., and Sakiyama-Elbert, S.E. Optimization of fibrin scaffolds for differentiation of murine embryonic stem cells into neural lineage cells. Biomaterials **27,** 5990, 2006.

10. Yim, E.K., and Leong, K.W. Proliferation and differentiation of human embryonic germ cell derivatives in bioactive polymeric fibrous scaffold. J Biomater Sci **16,** 1193, 2005.

11. Silver, J., and Miller, J.H. Regeneration beyond the glial scar. Nat Rev Neurosci **5,** 146, 2004.

12. Freier, T., Montenegro, R., Shan Koh, H., and Shoichet, M.S. Chitin-based tubes for tissue engineering in the nervous system. Biomaterials **26,** 4624, 2005.

13. Piotrowicz, A., and Shoichet, M.S. Nerve guidance channels as drug delivery vehicles. Biomaterials **27,** 2018, 2006.

14. Katayama, Y., Montenegro, R., Freier, T., Midha, R., Belkas, J.S., and Shoichet, M.S. Coil-reinforced hydrogel tubes promote nerve regeneration equivalent to that of nerve autografts. Biomaterials **27,** 505, 2006.

15. Tsai, E.C., Dalton, P.D., Shoichet, M.S., and Tator, C.H. Matrix inclusion within synthetic hydrogel guidance channels improves specific supraspinal and local axonal regeneration after complete spinal cord transection. Biomaterials **27,** 519, 2006.

16. Tsai, E.C., Dalton, P.D., Shoichet, M.S., and Tator, C.H. Synthetic hydrogel guidance channels facilitate regeneration of adult rat brainstem motor axons after complete spinal cord transection. J Neurotrauma **21,** 789, 2004.

17. Nomura, H., Katayama, Y., Shoichet, M.S., and Tator, C.H. Complete spinal cord transection treated by implantation of a reinforced synthetic hydrogel channel results in syringomyelia and caudal migration of the rostral stump. Neurosurgery **59,** 183, 2006.

18. Jimenez Hamann, M.C., Tsai, E.C., Tator, C.H., and Shoichet, M.S. Novel intrathecal delivery system for treatment of spinal cord injury. Exp Neurol **182,** 300, 2003.

19. Jimenez Hamann, M.C., Tator, C.H., and Shoichet, M.S. Injectable intrathecal delivery system for localized administration of EGF and FGF-2 to the injured rat spinal cord. Exp Neurol **194,** 106, 2005.

20. Gupta, D., Tator, C.H., and Shoichet, M.S. Fast-gelling injectable blend of hyaluronan and methylcellulose for intrathecal, localized delivery to the injured spinal cord. Biomaterials **27,** 2370, 2006.

21. Freier, T., Jimenez-Hamann, M., Katayama, Y., Musoke-Zawedde, P., Piotrowicz, A., Yuan, Y., Shoichet, M.S., and Midha, R. Biodegradable Polymers in Neural Tissue Engineering. Ames, IA: American Scientific Publishers, 2005.

22. Khor, E., and Lim, L.Y. Implantable applications of chitin and chitosan. Biomaterials **24,** 2339, 2003.

23. Hung, C.H., Lin, Y.L., and Young, T.H. The effect of chitosan and PVDF substrates on the behavior of embryonic rat cerebral cortical stem cells. Biomaterials **27,** 4461, 2006.

24. Zhao, F., Grayson, W.L., Ma, T., Bunnell, B., and Lu, W.W. Effects of hydroxyapatite in 3-D chitosan-gelatin polymer network on human mesenchymal stem cell construct development. Biomaterials **27,** 1859, 2006.

25. Zahir, T., Nomura, H., XiaoDong, G., Kim, H., Tator, C., Morshead, C., and Shoichet, M. Bioengineering neural stem/progenitor cell-coated tubes for spinal cord injury repair. Cell Transplant in press.

26. Namiki, J., and Tator, C.H. Cell proliferation and nestin expression in the ependyma of the adult rat spinal cord after injury. J Neuropathol Exp Neurol **58,** 489, 1999.

27. Mothe, A.J., and Tator, C.H. Proliferation, migration, and differentiation of endogenous ependymal region stem/progenitor cells following minimal spinal cord injury in the adult rat. Neuroscience **131,** 177, 2005.

28. Kojima, A., and Tator, C.H. Epidermal growth factor and fibroblast growth factor 2 cause proliferation of ependymal precursor cells in the adult rat spinal cord *in vivo*. J Neuropathol Exp Neurol **59,** 687, 2000.

29. Hofstetter, C.P., Holmstrom, N.A., Lilja, J.A., Schweinhardt, P., Hao, J., Spenger, C., Wiesenfeld-Hallin, Z., Kurpad, S.N., Frisen, J., and Olson, L. Allodynia limits the usefulness of intraspinal neural stem cell grafts; directed differentiation improves outcome. Nat Neurosci **8,** 346, 2005.

30. Ueki, T., Tanaka, M., Yamashita, K., Mikawa, S., Qiu, Z., Maragakis, N.J., Hevner, R.F., Miura, N., Sugimura, H., and Sato, K. A novel secretory factor, Neurogenesin-1, provides neurogenic environmental cues for neural stem cells in the adult hippocampus. J Neurosci **23,** 11732, 2003.

31. Song, H., Stevens, C.F., and Gage, F.H. Astroglia induce neurogenesis from adult neural stem cells. Nature **417,** 39, 2002.

32. Song, H.J., Stevens, C.F., and Gage, F.H. Neural stem cells from adult hippocampus develop essential properties of functional CNS neurons. Nature Neurosci **5,** 438, 2002.

33. Hakamata, Y., Tahara, K., Uchida, H., Sakuma, Y., Nakamura, M., Kume, A., Murakami, T., Takahashi, M., Takahashi, R., Hirabayashi, M., Ueda, M., Miyoshi, I., Kasai, N., and Kobayashi, E. Green fluorescent protein-transgenic rat: a tool for organ transplantation research. Biochem Biophys Res Commun **286,** 779, 2001.

34. Kulbatski, I., Mothe, A.J., Keating, A., Hakamata, Y., Kobayashi, E., and Tator, C.H. Oligodendrocytes and radial glia derived from adult rat spinal cord progenitors: morphological and immunocytochemical characterization. J Histochem Cytochem **55,** 209, 2007.

35. Morshead, C.M., Reynolds, B.A., Craig, C.G., McBurney, M.W., Staines, W.A., Morassutti, D., Weiss, S., and van der Kooy, D. Neural stem cells in the adult mammalian forebrain: a relatively quiescent subpopulation of subependymal cells. Neuron **13,** 1071, 1994.

36. Reynolds, B.A., and Weiss, S. Generation of neurons and astrocytes from isolated cells of the adult mammalian central nervous system. Science **255,** 1707, 1992.

37. Parr, A.M., Kulbatski, I., and Tator, C.H. Transplantation of adult rat spinal cord stem/progenitor cells for spinal cord injury. J Neurotrauma **24,** 835, 2007.

38. Mothe, A.J., Kulbatski, I., van Bendegem, R.L., Lee, L., Kobayashi, E., Keating, A., and Tator, C.H. Analysis of green fluorescent protein expression in transgenic rats for tracking transplanted neural stem/progenitor cells. J Histochem Cytochem **53,** 1215, 2005.

39. Tsai, E.C., Krassioukov, A.V., and Tator, C.H. Corticospinal regeneration into lumbar grey matter correlates with locomotor recovery after complete spinal cord transection and repair with peripheral nerve grafts, fibroblast growth factor 1, fibrin glue, and spinal fusion. J Neuropathol Exp Neurol **64,** 230, 2005.

40. Tsai, E.C., van Bendegem, R.L., Hwang, S.W., and Tator, C.H. A novel method for simultaneous anterograde and retrograde labeling of spinal cord motor tracts in the same animal. J Histochem Cytochem **49,** 1111, 2001.

41. Anthes, D.L., Theriault, E., and Tator, C.H. Ultrastructural evidence for arteriolar vasospasm after spinal cord trauma. Neurosurgery **39,** 804, 1996.

42. Spilker, M.H., Yannas, I.V., Kostyk, S.K., Norregaard, T.V., Hsu, H.P., and Spector, M. The effects of tubulation on healing and scar formation after transection of the adult rat spinal cord. Restor Neurol Neurosci **18,** 23, 2001.

43. Bunge, M.B. Bridging the transected or contused adult rat spinal cord with Schwann cell and olfactory ensheathing glia transplants. Prog Brain Res **137,** 275, 2002.

44. Ramon-Cueto, A., Cordero, M.I., Santos-Benito, F.F., and Avila, J. Functional recovery of paraplegic rats and motor axon regeneration in their spinal cords by olfactory ensheathing glia. Neuron **25,** 425, 2000.

45. Park, K.I., Liu, S., Flax, J.D., Nissim, S., Stieg, P.E., and Snyder, E.Y. Transplantation of neural progenitor and stem cells: developmental insights may suggest new therapies for spinal cord and other CNS dysfunction. J Neurotrauma **16,** 675, 1999.

46. Silva, G.A., Czeisler, C., Niece, K.L., Beniash, E., Harrington, D.A., Kessler, J.A., and Stupp, S.I. Selective differentiation of neural progenitor cells by high-epitope density nanofibers. Science **303,** 1352, 2004.

47. Lu, P., Jones, L.L., Snyder, E.Y., and Tuszynski, M.H. Neural stem cells constitutively secrete neurotrophic factors and promote extensive host axonal growth after spinal cord injury. Exp Neurol **181,** 115, 2003.

48. Itoh, S., Suzuki, M., Yamaguchi, I., Takakuda, K., Kobayashi, H., Shinomiya, K., and Tanaka, J. Development of a nerve scaffold using a tendon chitosan tube. Artif Organs **27,** 1079, 2003.

49. Rosales-Cortes, M., Peregrina-Sandoval, J., Banuelos-Pineda, J., Castellanos-Martinez, E.E., Gomez-Pinedo, U.A., and Albarran-Rodriguez, E. [Regeneration of the axotomised sciatic nerve in dogs using the tubulisation technique with Chitosan biomaterial preloaded with progesterone]. Rev Neurol **36,** 1137, 2003.

50. Rosales-Cortes, M., Peregrina-Sandoval, J., Banuelos-Pineda, J., Sarabia-Estrada, R., Gomez-Rodiles, C.C., Albarran-Rodriguez, E., Zaitseva, G.P., and Pita-Lopez, M.L. Immunological study of a chitosan prosthesis in the sciatic nerve regeneration of the axotomized dog. J Biomater Appl **18,** 15, 2003.

51. Yuan, Y., Zhang, P., Yang, Y., Wang, X., and Gu, X. The interaction of Schwann cells with chitosan membranes and fibers *in vitro*. Biomaterials **25,** 4273, 2004.

52. Taylor, R.M., Lee, J.P., Palacino, J.J., Bower, K.A., Li, J., Vanier, M.T., Wenger, D.A., Sidman, R.L., and Snyder, E.Y. Intrinsic resistance of neural stem cells to toxic metabolites may make them well suited for cell non-autonomous disorders: evidence from a mouse model of Krabbe leukodystrophy. J Neurochem **97,** 1585, 2006.

53. Doetsch, F. A niche for adult neural stem cells. Curr Opin Genet Dev **13,** 543, 2003.

54. Wiese, C., Rolletschek, A., Kania, G., Navarrete-Santos, A., Anisimov, S.V., Steinfarz, B., Tarasov, K.V., Brugh, S.A., Zahanich, I., Ruschenschmidt, C., Beck, H., Blyszczuk, P., Czyz, J., Heubach, J.F., Ravens, U., Horstmann, O., St-Onge, L., Braun, T., Brustle, O., Boheler, K.R., and Wobus, A.M. Signals from embryonic fibroblasts induce adult intestinal epithelial cells to form nestin-positive cells with proliferation and multilineage differentiation capacity *in vitro*. Stem Cells **24,** 2085, 2006.

55. McDermott, K.W., Barry, D.S., and McMahon, S.S. Role of radial glia in cytogenesis, patterning and boundary formation in the developing spinal cord. J Anat **207,** 241, 2005.

56. Wu, D., Miyamoto, O., Shibuya, S., Mori, S., Norimatsu, H., Janjua, N.A., and Itano, T. Co-expression of radial glial marker in macrophages/microglia in rat spinal cord contusion injury model. Brain Res **1051,** 183, 2005.

57. Li, H., Babiarz, J., Woodbury, J., Kane-Goldsmith, N., and Grumet, M. Spatiotemporal heterogeneity of CNS radial glial cells and their transition to restricted precursors. Dev Biol **271,** 225, 2004.

58. Kivirikko, K.I. Collagens and their abnormalities in a wide spectrum of diseases. Ann Med **25,** 113, 1993.

59. Prockop, D.J., and Kivirikko, K.I. Collagens: molecular biology, diseases, and potentials for therapy. Annu Rev Biochem **64,** 403, 1995.

60. Myllyharju, J., and Kivirikko, K.I. Collagens, modifying enzymes and their mutations in humans, flies and worms. Trends Genet **20,** 33, 2004.

61. Boot-Handford, R.P., Tuckwell, D.S., Plumb, D.A., Rock, C.F., and Poulsom, R. A novel and highly conserved collagen (pro(alpha)1(XXVII)) with a unique expression pattern and unusual molecular characteristics establishes a new clade within the vertebrate fibrillar collagen family. J Biol Chem **278,** 31067, 2003.

62. Byers, P.H. Folding defects in fibrillar collagens. Philos Trans R Soc Lond **356,** 151, 2001.

63. Boot-Handford, R.P., and Tuckwell, D.S. Fibrillar collagen: the key to vertebrate evolution? A tale of molecular incest. Bioessays **25,** 142, 2003.

64. Myllyharju, J., and Kivirikko, K.I. Collagens and collagen-related diseases. Ann Med **33,** 7, 2001.

65. Klapka, N., Hermanns, S., Straten, G., Masanneck, C., Duis, S., Hamers, F.P., Muller, D., Zuschratter, W., and Muller, H.W. Suppression of fibrous scarring in spinal cord injury of rat promotes long-distance regeneration of corticospinal tract axons, rescue of primary motoneurons in somatosensory cortex and significant functional recovery. Eur Neurosci **22,** 3047, 2005.

66. Klapka, N., and Muller, H.W. Collagen matrix in spinal cord injury. J Neurotrauma **23,** 422, 2006.

67. Iseda, T., Nishio, T., Kawaguchi, S., Kawasaki, T., and Wakisaka, S. Spontaneous regeneration of the corticospinal tract after transection in young rats: collagen type IV deposition and astrocytic scar in the lesion site are not the cause but the effect of failure of regeneration. J Comp Neurol **464,** 343, 2003.

68. Liesi, P., and Kauppila, T. Induction of type IV collagen and other basement-membrane-associated proteins after spinal cord injury of the adult rat may participate in formation of the glial scar. Exp Neurol **173,** 31, 2002.

69. Yoshii, S., Oka, M., Shima, M., Taniguchi, A., Taki, Y., and Akagi, M. Restoration of function after spinal cord transection using a collagen bridge. J Biomed Mater Res **70,** 569, 2004.

70. Yoshii, S., Oka, M., Shima, M., Taniguchi, A., and Akagi, M. Bridging a 30-mm nerve defect using collagen filaments. J Biomed Mater Res **67,** 467, 2003.

71. Joosten, E.A., Veldhuis, W.B., and Hamers, F.P. Collagen containing neonatal astrocytes stimulates regrowth of injured fibers and promotes modest locomotor recovery after spinal cord injury. J Neurosci Res **77,** 127, 2004.

72. Schwab, M.E. Nogo and axon regeneration. Curr Opin Neurobiol **14,** 118, 2004.

Address reprint requests to:
Charles H. Tator, M.D., Ph.D.
Toronto Western Research Institute
Toronto Western Hospital and University of Toronto
Room 12–435, McLaughlin Wing
399 Bathurst Street
Toronto ON M5T 2S8
Canada

E-mail: charles.tator@uhn.on.ca